

Hydrothermal synthesis of copper powder with varied morphologies via copper(II) reduction with multidentate H₄Pmida ligand and its application for Cu-Ni foam electrode for supercapacitors

Yan-Fang Duan, Li-Yan Tian, Ping-Ping Sun, Fa-Nian Shi*

Key Laboratory of Polymer and Catalyst Synthesis Technology of Liaoning Province, School of Environmental and Chemical Engineering, Shenyang University of Technology, Shenyang 110870, China

*E-mail: yf.duan@foxmail.com; tianliyan@smail.sut.edu.cn; sppsunny@foxmail.com

Received: 7 February 2021 / Accepted: 22 March 2021 / Published: 30 April 2021

Micro-sized copper particles showing distinct morphologies were prepared via reduction of the Cu (II) salt by N-(Phosphonomethyl)iminodiacetic acid (H₄Pmida) using a hydrothermal treatment method. Copper was identified as the single phase in the several powders prepared attesting the feasibility of the method to obtain the pure metal phase. The key role of H₄Pmida to modify the particles morphology and the plausible mechanism involved are discussed. The in situ as-prepared Cu on Ni foam was used as electrode materials of supercapacitors which showed the interesting electrochemical performance regulated by the pressure employed during the electrode preparation.

Keywords: Copper; Hydrothermal treatment; Micro-sized particle; H₄Pmida; Morphology; Supercapacitor.

1. INTRODUCTION

The last decade has seen a strong development on the rational design and chemical synthesis of functional materials, in principle avoiding extreme conditions of temperature and pressure. Many studies have been carried out to mold the size and shape of well-known inorganic particulates, paving the way to new applications such as in the context of nanotechnologies. For example, due to interesting size dependent physical properties, ubiquitous metal copper has been investigated due to potential applications as an interconnect material on micro- and nano-circuitry [1]. Contrasting to other metals, such as gold and silver, studies on the morphological modification of micro- and nano-sized metallic copper have been very limited.

In aqueous solution, the reduction of common Cu(II) salts, in mild conditions, tends to yield the Cu₂O phase [2, 3]. So far, synthetic methods employed to obtain well-defined copper particles involves

a high-temperature (CVD or laser), electrochemical procedures, reduction in aqueous solution with a reductant such as N_2H_4 , or simple reduction with organic solvents [4-7]. In fact, H_4Pmida (Scheme 1) is a strong chelating multidentate ligand containing one N atom, two carboxyl groups and one phosphonate organic functional group, which often easy form several stable 5-member rings when linking metal centers [8-16]. However, the N atom in H_4Pmida ligand is very much easy to be oxidized, thus, Cu-Pmida coordination complexes can be obtained only at room temperature [17] or under mild hydrothermal conditions (100 °C) [18], otherwise, H_4Pmida ligand will be oxidized by Cu^{2+} and consequently metal copper obtained via well designed mild hydrothermal treatment as seen in this work.

Recently, we have conducted several researches on supercapacitors with the electrodes using different materials such as the NiO/C&S composite [19], the hollow $NiCo_2O_4/NiO$ oxide composite [20] and the transition metal coordination polymers [21-23], as a continuous work in the area of supercapacitors, we now extend the study of capacitor energy storage properties to copper metal.

Herein, a varied hydrothermal method to synthesize morphological well-defined Cu particles was described with H_4Pmida as a reducing reagent. It was found, for the case of copper (II), that the metallic phase could be easily obtained in the experimental conditions used. Noteworthy, the metal phase appeared as well-defined particles when the H_4Pmida ligand was present. This led us to investigate the synthetic method in more detail, particularly the role of H_4Pmida as a key mediator in the synthesis of well-defined copper particles. Micro sized Cu particles were well attached on the surface of nickel foam and showed interesting electrochemical performance as supercapacitors electrode material.

2. EXPERIMENTAL

2.1 Materials

All chemicals used were from commercial sources without further purification. N-(phosphonomethyl)iminodiacetate acid hydrate (H_4Pmida , $C_5H_{10}NO_7P$, 97% Fluka), copper (II) acetate monohydrate ($Cu(Ac)_2 \cdot H_2O$, 98% Panreac), cerous chloride heptahydrate ($CeCl_3 \cdot 7H_2O$, 98.5% Fluka) and diethylenetriamine ($(NH_2CH_2CH_2)_2NH$, BDH Chemicals Ltd.). The homogeneous mixtures prepared were placed into 40 mL Teflon-lined autoclave. The reactions were kept at 140 °C or 100°C for 5 days in an oven and then the autoclaves were removed and slowly cooled to room temperature.

2.2 Synthesis of copper micro-particles

A mixture of H_4Pmida (0.680 g) and $Cu(Ac)_2 \cdot H_2O$ (0.800 g) in 18 g of distilled water was stirred thoroughly to homogeneity at ambient temperature and then placed in an autoclave. After reaction at 140 °C for 5 days, metallic copper particles were isolated by filtering the reacting solution. The final product was washed with distilled water using an ultrasound bath and air dried at room temperature. The pH (~5.2) of the solution was varied by adding 0.510 g of NaOH to the starting mixture.

2.3 Synthesis of copper micro-sheets

A similar procedure as above mentioned was employed but carrying out the reactions at 140 °C or even at 100 °C over 5 days under the pH of ~1.4 without adding NaOH for the pH adjustment.

2.4 Synthesis of copper micro-wires

A mixture of H₄Pmida (0.34 g), Cu(Ac)₂·H₂O (0.20 g), CeCl₃·7H₂O (0.25 g), and (NH₂CH₂CH₂)₂NH (0.10 g) in 18 g of distilled water was stirred thoroughly to homogeneity at ambient temperature and then placed in an autoclave. After reaction at 140°C for 5 days, metal copper wires were separated from the final solution by filtering. This product was then washed with distilled water using an ultrasound bath and air dried at room temperature.

2.5 Materials Characterization

SEM (scanning electron microscopy) and EDS (energy dispersive analysis of X-rays spectroscopy) were performed using a Hitachi S-4100 field emission gun tungsten filament instrument working at 25 kV. Powder X-ray diffraction (PXRD) was carried out using a X'Pert MPD Philips diffractometer (Cu-K_α radiation) with a curved graphite monochromator.

2.6 Capacitor preparation

In this experiment, metal copper was designed to grow on Ni foam by direct hydrothermal method. H₄Pmida, CuSO₄·5H₂O and LiOH·H₂O were weighed with an analytical balance in a molar ratio of 1:1:4, put into a 25ml reactor, ~4.0 g of distilled water was added, stirred magnetically for 30 minutes, then a quantitative amount of foamed nickel was put into the reactor, and made the foamed nickel completely to be soaked in the solution. The reactor was placed in an oven and reacted at a constant temperature for 3 days at 100°C. After the reactions were completed, the temperature was cooled down to the room temperature naturally, suction filtration, washing, and the cleaned foamed nickel was placed in a vacuum drying oven and dried at 60°C for 9 hours.

The CV and GCD tests were carried out under a three-electrode system for two supercapacitor electrodes by compressing the electrode sheets at the pressures of 10 MPa and 2 MPa, respectively, for 10 seconds.

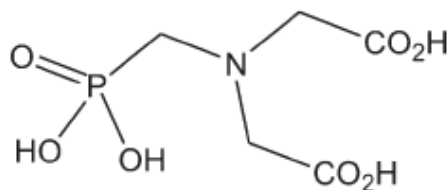
2.7 Electrochemical measurements

The foam nickel-loaded copper electrodes were pressed under 2 MPa under the ambient conditions. The electrochemical properties of the as-prepared copper electrode (1×1cm) were tested in a three-electrode system with Pt foil and Hg/HgCl working as the counter electrode and reference electrode, respectively. KOH aqueous solution (6M) was used as the electrolyte. The

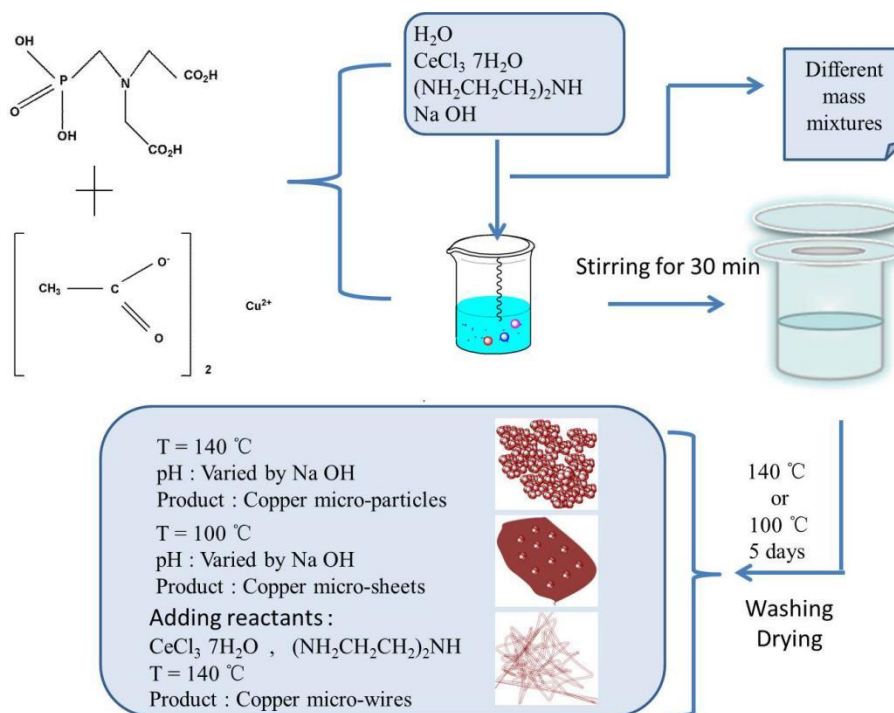
electrochemical performance of the electrode was evaluated by cyclic voltammetry (CV), galvanostatic charge–discharge (GCD) and electrochemical impedance spectroscopy (EIS) employing a CHI660E (Chenhua, Shanghai, China) electrochemical workstation. While on the LAND CT2001 test system, the cyclic stability of the foam nickel-loaded copper electrode was studied by repeated the performance of charge and discharge cycles at a current density of 8 mA g^{-1} .

3. RESULTS AND DISCUSSION

Micro-sized copper particles with different morphologies are readily obtained via hydrothermal reactions in the presence of H_4Pmida (Scheme 1), which is a strong reducing agent and good chelating ligand for reactions with vanadium oxide (V) in aqua solution [24, 25].



Scheme 1. the molecular structure of H_4Pmida .



Scheme 2. Diagram of the procedures for the fabrication of metal copper products in different morphologies

While based on our experiments of reacting with Cu^{2+} salt, H_4Pmida ligand is only able to

reduce Cu^{2+} under hydrothermal conditions above 100 °C. A series of relevant reactions (Scheme2) were designed and performed in order to understand better how reaction conditions such as temperature, pH value of aqueous solution, and different starting reactants influence the formation of metallic copper, respectively.

Six important reactions were chosen to summarize in table 1. It is obviously that H₄Pmida ligand can reduce Cu^{2+} ions into metallic copper (Cu^0), for our cases, in the absence of other starting materials such as $\text{CeCl}_3 \cdot 7\text{H}_2\text{O}$ and $(\text{NH}_2\text{CH}_2\text{CH}_2)_2\text{NH}$, even at 100 °C under acidic condition. Based on our experimental results, when the reaction took place at 140 °C, pH values for these reducing reactions can be varied from 1 to 5 suggesting small affection of pH value to the Pmida-reducing hydrothermal reactions, while at 100 °C, pH value became crucial for the formation of metallic copper. When pH value was high up to 5, at 100 °C Pmida could not reduce Cu^{2+} into Cu and only Cu_2O was obtained as a mono-phase (table 1 and figure 1e). The final products were clearly proved by powder XRD patterns (figure 1), of which figure 1a-d index well in cubic copper structure with *Fm3m* space group [26]. There is not any extra-peak of Cu_2O or CuO impurities in these PXRD patterns, while figure 1e matches well with known Cu_2O phase without copper metal phase due to the relative high pH and low reaction temperature (100 °C).

Table 1. Reaction conditions and results of Pmida and $\text{Cu}(\text{Ac})_2$ as starting reactants

codes	T [°C]	pH	final color of water	product & color	morphology
Cu-Pmida1	140	1.4	brown	copper, pink	sheets & particles
Cu-Pmida2*	140	5.2	brown	copper, pink	particles
Cu-Pmida3	100	1.4	greenish blue	copper, pink	sheets & particles
Cu-Pmida4*	100	5.2	blue	Cu_2O , purple	particles
Cu-Pmida5**	140	3.9	brown	copper, pink	micro-wires
Cu-Pmida6**	140	3.5	dark brown	copper, pink	particles

Note: * pH value were adjusted with NaOH reagent; ** Cu-Pmida5 with $\text{CeCl}_3 \cdot 7\text{H}_2\text{O}$ + $(\text{NH}_2\text{CH}_2\text{CH}_2)_2\text{NH}$ and Cu-Pmida6 only with $(\text{NH}_2\text{CH}_2\text{CH}_2)_2\text{NH}$.

Figure 2 shows the SEM images of Cu particles. In acidic conditions, Cu particles are grown in a rough spherical appearance (figure 2a) with an average diameter range of 8 μm , while pH approaches to neutral (pH=5.2), Cu particles are grown in hexagonal geometry and their appearances are well kept with the sizes of particles varied in the range from 4 μm to 6 μm (figure 2b). Figure 3 exhibits a typical SEM image of a bulk Cu sheet in an irregular shape and rough surface. The sheet seems to be built up with blocks of Cu particles (figure 3 inset). the shapes of Cu particles are very distorted and the fringes of the interfaces of each two neighboring Cu particles are highly irregular and jagged owing to the strong pushed and squeezed force derived from the insitu reduction of Cu^{2+} ions by Pmida ligand. Figure 4a displays a SEM image of the mass Cu wires. Some of them are grown in a uniform shape like ropes, others are grown with two much thicker ends, while the rest are with one thicker end like tadpoles with a long tail (figure 4). These irregular wires are easily and naturally bended without any

fracture. The sizes of Cu wires are varied from 20 μm to 5 μm in diameters and from about 2 mm to 0.6 mm in length.

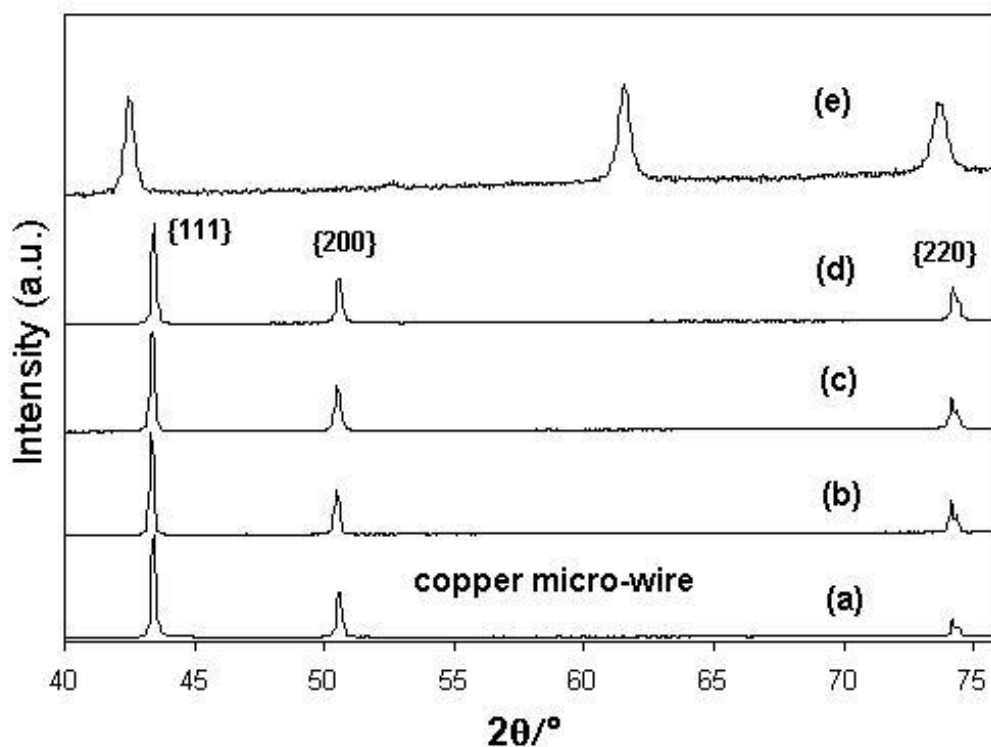


Figure 1. PXRD patterns of the final products from the reactions with (a) 140 °C, pH=3.9 coded as Cu-Pmida5 in table 1; (b) at 140 °C, pH=1.4; (c) at 140 °C, pH=5.2; (d) at 100 °C, pH=1.4; and (e) at 100 °C, pH=5.2, and the pattern fits well with Cu_2O phase.

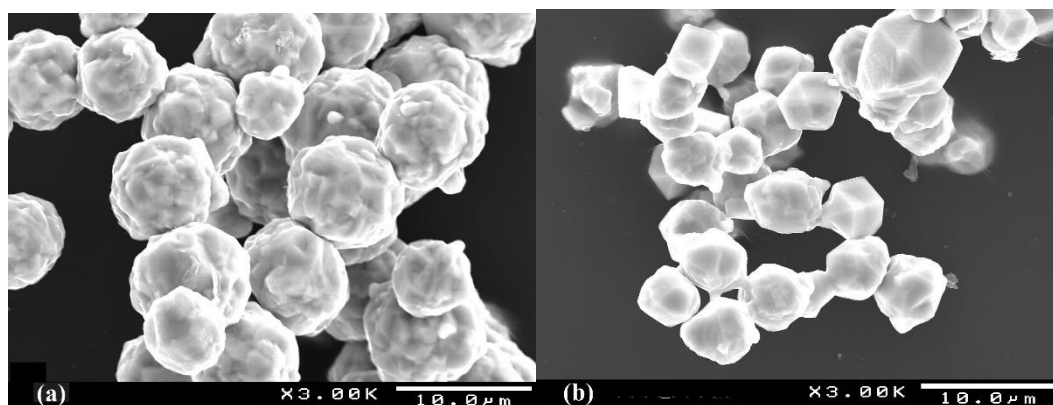


Figure 2. SEM images of the samples obtained at 140 °C. (a) Rough spherical copper metal particles synthesized via pH=1.4; (b) Well shaped polyhedra copper metal particles synthesized via pH=5.2.

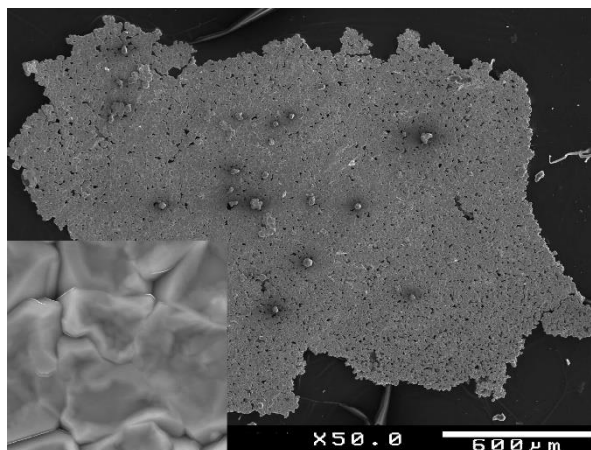


Figure 3. A typical SEM image of the copper porous sheet. Inset shows particles jam-packed into the sheet, the bar is of 10.0um.

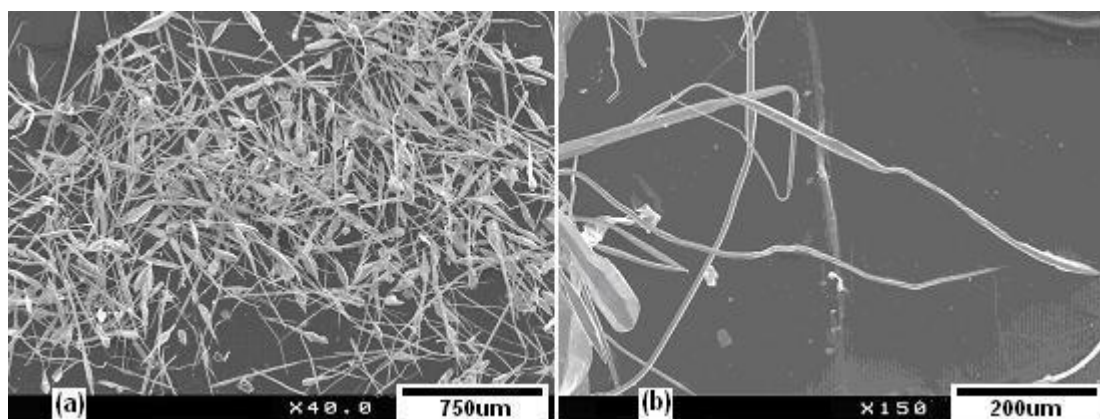


Figure 4. SEM images of the copper wires. (a) a typical image of the mass Cu wires in low magnification; (b) Cu wire image with higher magnification showing the features of irregular shapes, naturally bending and about 1 mm long.

Although the direct evidence has not been gained yet to prove how the morphological modification took place during the formation process of different morphological copper metal, especially to forming copper micro-wires, some important clues can also lead us to some useful assumption to understand somewhat the formation mechanism. In our cases, it is clearly that the hydrothermal process of Cu^{2+} ions reduced by H_4Pmida ligand is an in-situ reduction. Under the reaction conditions mentioned above, the morphological structural features of metallic copper were determined by those of the precursors that usually called intermediate phases such as Cu-Pmida complex and some unknown complexes (It might be a certain Ce-Cu-Pmida complex in the case for Cu wire). So we consider, for example, certain unknown complex as a precursor to form copper wire might have original one dimensional chain appearance, of which was indirectly confirmed by the SEM image and EDS spectrum (figure 5). In fact, in order to confirm such a speculation, we did a synthetic experiment (table 1: Cu-Pmida 6) without adding $\text{CeCl}_3 \cdot 7\text{H}_2\text{O}$ as the initial reaction reagent, but using

$(\text{NH}_2\text{CH}_2\text{CH}_2)_2\text{NH}$. The experimental result shows only copper metal particles were obtained suggesting that the presence of $\text{CeCl}_3 \cdot 7\text{H}_2\text{O}$ is a key factor for the formation of copper micro-wires and the long rod-shaped multi-textured substance shown in figure 6 (Ce-Cu-Pmida) may be an intermediate in the in situ redox reaction for the formation of copper wires. Now much effort has been being taken to grow single crystals of such mediate Ce-Cu-Pmidacompound at low temperature.

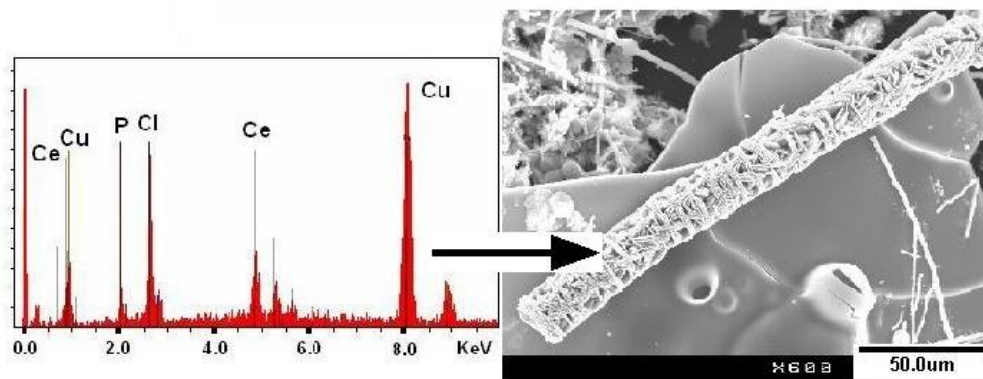


Figure 5. EDS spectrum and SEM image of a rope-like unknown complex precursor as intermediate obtained via hydrothermal reaction at 100°C for 5 days by using H_4Pmida , $\text{CeCl}_3 \cdot 7\text{H}_2\text{O}$ and $\text{Cu}(\text{Ac})_2 \cdot \text{H}_2\text{O}$ as starting materials.

Using H_4Pmida acid, copper salt and nickel foam, under mild hydrothermal conditions, metal copper powder is obtained and spreads very evenly on the surface of foamed nickel. Under the optical microscope (figure 6a) original gray nickel foam has now become a uniform bright brown metallic copper indicating the successful reduction of copper ions (Cu^{2+}) into metal copper particles (Cu^0) on the surface of nickel foam. Under the electron microscope magnified 800 times, the surface of the reticulated foamed nickel is covered with large numbers of copper particles with the appearance of a uniform polyhedron (figure 6b) showing copper particles ranging in size from about 20 micrometers to a few micrometers. Such a metal copper-loaded foamed nickel is assembled into a supercapacitor for the following electrochemical tests.

The CV curves (figure 7a and b) were obtained when the scan rate of 10mV s^{-1} , 20mV s^{-1} , 30mV s^{-1} , 50mV s^{-1} , 80mV s^{-1} , 100mV s^{-1} , 130mV s^{-1} and 150mV s^{-1} . The electrode for figure 7a was pressed at 10MPa, which shows distinct oxidation peaks, but the reduction peaks are not obvious. While the electrode for figure 7b was pressed at 2MPa. It can be seen there are two couple of redox peaks in this figure, which are a unique feature of super capacitors [27]. The above CV data indicate that the electrode under the pressure of 2MPa has better reversibility than the one under 10MPa. With increasing the scan rate, it is obvious that the current response increases with the increase of scan rates and the enclosed areas become wider with the fine shape of the curve residual, and the shapes of CV curves remains unchanged, suggesting the well-matched configuration of the electrodes and a good rate capability [27-29].

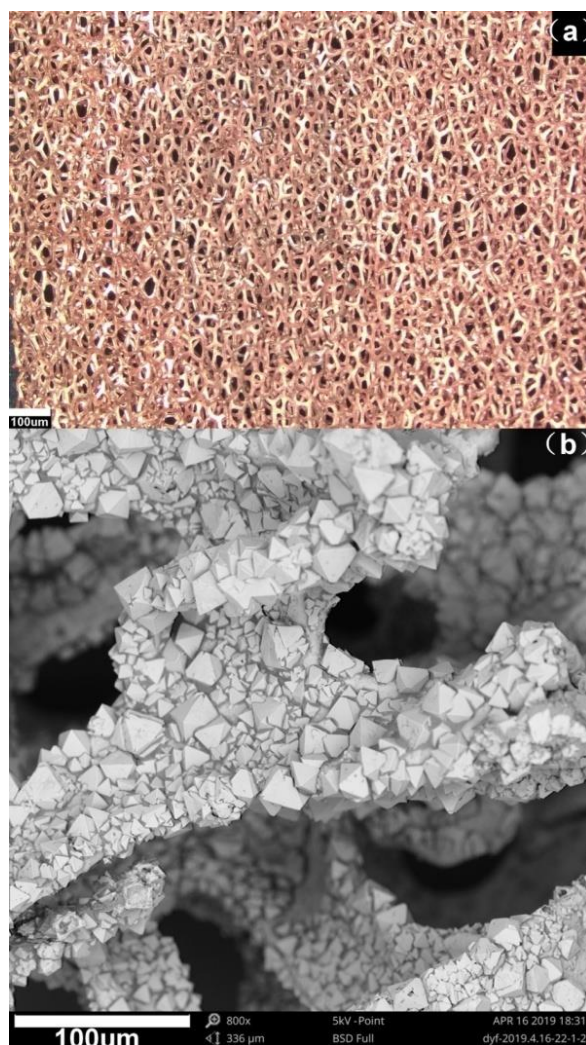


Figure 6. (a) Colorful optical image of copper metal spreading on a Ni foam showing a uniform reddish-brown copper layer on the surface of Ni foam; (b) A SEM image of the Ni foam under high magnification displaying copper particles coated on the surface of Ni foam

Figure 7c is a GCD test performed on the same copper electrode sheet pressed at a pressure of 10MPa, and the charge-discharge time is almost the same. The specific capacitance of this electrode is $41.67F\ g^{-1}$ when the current density of $1A\ g^{-1}$. Whereas figure 7d shows the GCD curve of the electrode at the pressure of 2MPa. As the current density increases, all GCD curves have similar shapes and platforms. This phenomenon is caused by the redox reaction between the electrode/electrolyte interface [30-32], which is a typical characteristic of Faraday reaction at the electrode/electrolyte interface [33]. As shown in figure 7d, when the current density is $1A\ g^{-1}$, linear behavior appears, along with a long discharging time, demonstrating that all the active sites contributed to the charge storage[29]. The specific capacitance is $111.11F\ g^{-1}$ at a current density of $1A\ g^{-1}$, which is higher than the specific capacitance ($41.67F\ g^{-1}$) of the capacitor electrode of the Cu-Ni foam prepared at the pressure of 10MPa. It is proved that different pressures affect the electrochemical performance, thus finding the suitable pressure on electrode is very important for the preparation of the capacitor electrode with good quality.

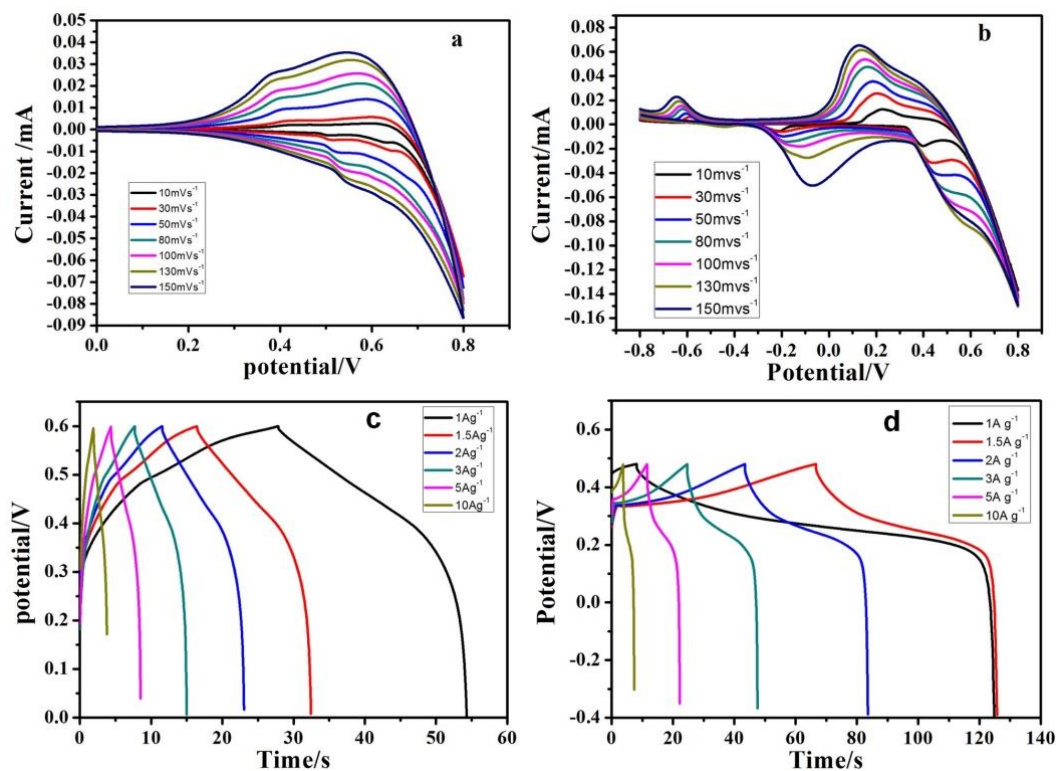


Figure 7. (a) The CV curves of the copper electrode pressed at 10MPa; (b) The CV curves of the copper electrode pressed at 2MPa; (c) The GCD plots of the copper electrode pressed at 10MPa; (d) The GCD plots of the copper electrode pressed at 2MPa.

The binder-free self-growing micron Cu-Ni foam prepared in this study was compared with the previous reported material (table 2). It can be seen that this material shows certain advantages at high current density, and it has a great research prospect. This advantage may be due to self-assembled and in situ grows material, which have not any influence of binder.

Table 2. Comparison of the specific capacitance with previous works.

Materials	Specific capacitance (GCD)	Stability (%) (cycle)	Reference.
CuS	237 F g ⁻¹ (0.5 A g ⁻¹)	88 % (4000 cycles)	34
Ni-Zn/TiO ₂ nanotubes	325 F g ⁻¹ (0.45 mA cm ⁻²)	-	35
NPC ₆₅₀	222 F g ⁻¹ (50 mA g ⁻¹)	-	36
Ni-Co MOF	173 F g ⁻¹ (0.5 A g ⁻¹)	-	37
Ni-Cu foam	536 F g ⁻¹ (1 A g ⁻¹)	81.8 % (3000 cycles)	38
Al doped MnO ₂	213 F g ⁻¹ (0.1 A g ⁻¹)	-	39
Ni-Cu foam	105 F g ⁻¹ (1 mA cm ⁻²)	90 % (10000 cycles)	40
Ni-MOF/CNT//rGO/C ₃ N ₄	103 F g ⁻¹ (0.5A g ⁻¹)	95 % (5000 cycles)	41
Cu-Ni foam	111.11 F g ⁻¹ (1 A g ⁻¹)	80 % (1000 cycles)	This work

The Nyquist diagram of Cu-Ni Foam electrode in the frequency range of 0.1Hz to 100kHz is shown in figure 8a, consisting of a semicircle at high frequencies and a straight line at low frequencies. The diameter of the semicircles represents the charge transfer resistance at the electrode-electrolyte interface, and the straight line represents the diffusion characteristics of electrolyte on the electrode surface[42], The test potential voltage range is between 0.0-0.7 V. The low resistance ($R_s = 0.74\Omega$) in the figure indicates a high conductivity between the copper electrode and the electrolyte. In the high frequency region, the smaller semicircular arc represents the fast process in dynamics [43], the real intercept is small. Because of the small charge transfer resistance ($R_{ct} = 1.74\omega$), it shows that the charge of the copper electrode is fast moving. In the low frequency region, the impedance curve is sharp, almost parallel to the imaginary axis, and tends to be close to the vertical line, indicating that the foam nickel-copper electrode exhibits the characteristics of ideal capacitance behavior[44].

In order to evaluate the practical application of the copper electrode materials for supercapacitors, we have test the cycling stability. Unlike other supercapacitors, the retention decreases sharply during the first few cycles, and after the small fluctuation, the retention rate tends to stabilize at the 80th cycle (figure 8b). After 1000 cycles, the capacitance retention of the copper electrode is still maintained at around 80% (figure 8b), which indicates that the electrode material has good cyclic stability.

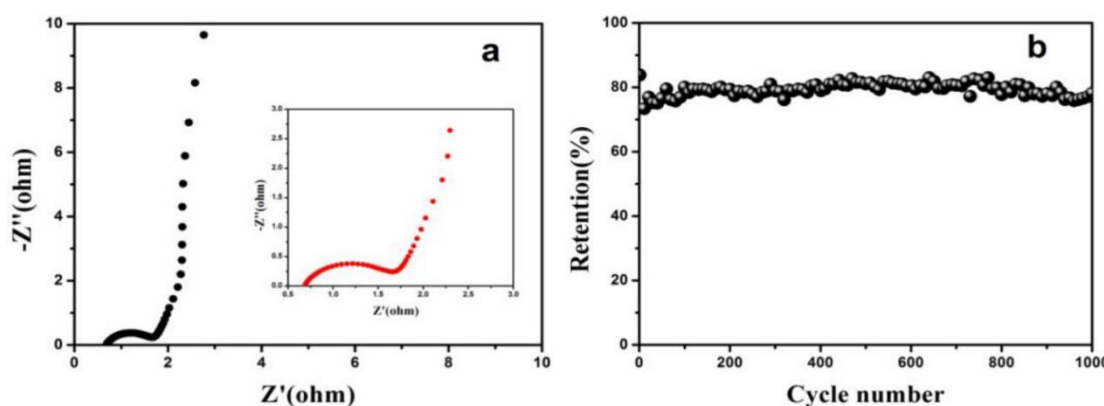


Figure 8. (a) The Nyquist plot of the foam nickel-loaded copper electrode; (b) The capacitor cycling stability of the foam nickel-loaded copper electrode.

4. CONCLUSIONS

In summary, uniformed micro-sized crystalline metal copper with various morphologies has obtained in large yield by mild hydrothermal reactions of N-(phosphonomethyl)iminodiacetic acid (H_4Pmida) as a key mediator with Cu^{2+} salt. Powder XRD patterns and EDS spectra confirm the phase purification, while SEM images clearly prove the presence of different morphologies of copper such as wires, sheets and particles. This work provides a simple and controllable route to the formation of metallic copper in presence of Cu^{2+} salts as oxidant and H_4Pmida as a reducing agent under the hydrothermal conditions. In addition, the more important point is that through the hydrothermal process by using different complexes as precursors, metallic copper can be designably modified to

form different morphologies.

Furthermore, the metallic copper is uniformly in situ attached to the foam nickel obtained by the one-step hydrothermal treatment. The as-prepared Cu-Ni bi-components is used as an electrode of the supercapacitor to obtain an interesting electrochemical property. The electrochemical performances (111.11F g^{-1} at 1A g^{-1}) of the supercapacitor prepared under low pressure (2MPa) conditions are much better than that (41.67F g^{-1} at 1A g^{-1}) prepared under high pressure (10MPa) conditions.

ACKNOWLEDGEMENT

Authors acknowledge the project 21571132 supported by the NSFC. This work was also supported by the key project (LZGD2017002) of Department of Education of Liaoning Province.

References

1. V. Champagne, D. Helfritsch, E. Wienhold and J. DeHaven, *J. Micromech. Microeng.*, 23 (2013) 065023-7.
2. Z. Wang, X. Chen, J. Liu, M. Mo, L.S. Yang and Y. Qian, *Solid State Commun.*, 130 (2004) 585.
3. L.Gou, C.J.F. Murphy, *J. Mater. Chem.*, 14 (2004) 735.
4. M.S. Polyakov, A.M. Badalyan, V.V. Kaichev and I.K. Igumenov, *Chem. Vapor. Depos.*, 20 (2014) 170.
5. Z. She, A. DiFalco, G. Hähner and M. Buck, *Beilstein J. Nano technol.*, 3 (2012) 101.
6. V. Andal, G. Buvaneswari. *J. Nano Res.*, 15 (2011) 11.
7. D. Xu, Y. Bai, Z. Li, Y. Guo and L. Bai, *Colloid. Surface. A*, 548 (2018) 19.
8. F.A. Almeida Paz, F.N. Shi, J. Klinowski, J. Rocha and T. Trindade, *Eur. J. Inorg. Chem.*, 2004 (2004) 2759.
9. F.A. Almeida Paz, F.N. Shi, L. Mafra, A. Makal, K. Wozniak, T. Trindade and J. Rocha, *Acta Crystallogr. E*, 61 (2005) m1628.
10. F.A. Almeida Paz, J. Rocha, J. Klinowski, T. Trindade, F.N. Shi and L. Mafra, *Prog. Solid. State Chem.*, 33 (2005) 113.
11. F.N. Shi, F.A. Almeida Paz, P.I. Girginova, L. Mafra, V.S. Amaral, J. Rocha, A. Makal, K. Wozniak, J. Klinowski and T. Trindade. *J. Mol. Struct.*, 754 (2005) 51.
12. F.N. Shi, F.A. Almeida Paz, P. Girginova, J. Rocha, V.S. Amaral, J. Klinowski and T. Trindade, *J. Mol. Struct.*, 789 (2006) 200.
13. F.N. Shi, F.A. Almeida Paz, P.I. Girginova, V.S. Amaral, J. Rocha, J. Klinowski and T. Trindade. *Inorg. Chim. Acta*, 359 (2006) 1147.
14. L. Mafra, F.A. Almeida Paz, F.N. Shi, J. Rocha, T. Trindade, C. Fernandez, A. Makal, K. Wozniak and J. Klinowski, *Chem. Eur. J.*, 12 (2006) 363.
15. T.H. Yang, A.R. Silva, L. Fu and F.N. Shi, *Dalton Trans.*, 44 (2015) 13745.
16. H.L. Chang, Y.W. Bai, X.Y. Song, Y.F. Duan, P.P. Sun, B. Tian, G.M. Shi, H.P. You, J. Gao and F.N. Shi, *Electrochim. Acta.*, 321 (2019) 134647.
17. F.A. Almeida Paz, F.N. Shi, T. Trindade, J. Klinowski and J. Rocha. *Acta Crystallogr. E*, 61 (2005) m2247.
18. F.N. Shi, F.A. Almeida Paz, T. Trindade and J. Rocha, *Acta Crystallogr. E*, 62 (2006) m335.
19. F.N. Shi, J. Jiang, H. Xiao and X. Li, *Mater. Des.*, 153 (2018) 203.
20. P.P. Sun, Y.H. Zhang, X. Yu, Q. Shi, B. Tian, J. Gao and F.N. Shi, *J. Alloys Compd.*, 832 (2020) 154954.
21. P.P. Sun, Y.H. Zhang, X. Yu, Q. Shi, B. Tian, J. Gao and F.N. Shi. *Inorg. Chim. Acta*, 508 (2020) 119629.

22. J.J. Xing, P.P. Sun, Y.H. Zhang and F.N. Shi, *Inorg. Chim. Acta*, 517 (2020) 120197.
23. P.P. Sun, Y.H. Zhang, J. Mu, B. Tian and F.N. Shi, *Inorg. Chem. Commun.*, 125 (2021) 108436.
24. D.C. Crans, F.L. Jiang, I. Boukhobza, I. Bodi and T. Kiss, *Inorg. Chem.*, 38 (1999) 3275.
25. D.P. Riley, D.L. Fields, W. Rivers, *Inorg. Chem.*, 30 (1991) 4191.
26. H.M. Otte, *J. Appl. Phys.*, 32 (1961) 1536.
27. D. Wang, H.Q. Li, X.L. Zhang, P. Ding and Y.F. Deng, *Surf. Coat. Technol.*, 403 (2020) 126406.
28. H.Y. Liu, Z.Y. Guo, S.B. Wang, X.C. Xun, D. Chen and J.S. Lian, *J. Alloys Compd.*, 846 (2020) 156504.
29. S. Alipour, M. Arvand. *Colloid. Surface. A*, 606 (2020) 125456.
30. C.X. Lu, A.R. Li, T.F. Zhai, C.R. Niu, H.P. Duan, L. Guo and W. Zhou, *Energy Stor. Mater.*, 26 (2020) 472.
31. Y.X. Liu, Y.Z. Wang, H.Q. Wang, P.H. Zhao, H. Hou and L. Guo, *Appl. Surf. Sci.*, 492 (2019) 455.
32. S.W. Fang, J. Li, C.L. Xiang, Y.J. Zou, F. Xu, L.X. Sun and J. Zhang. *J. Alloys Compd.*, 845 (2020) 156024.
33. J.S. Xu, Y.D. Sun, M.J. Lu, L. Wang, J.H. Zhang, J. Qian and X.Y. Liu, *Chem. Eng. J.*, 334 (2018) 1466.
34. J. Zhang, H. Feng, J. Yang, Q. Qin, H.M. Fan, C.Y. Wei and W.J. Zheng, *ACS Appl. Mater. Inter.*, 39 (2015) 21735.
35. F. Gobal, M. Faraji, *Electrochim. Acta*, 100 (2013) 133.
36. B. Liu, H. Shioyama, H.L. Jiang, X.B. Zhang and Q. Xua, *Carbon*, 48 (2010) 456.
37. C.J. Ye, Q.Q. Qin, J.Q. Liu, W.P. Mao, J. Yan, Y. Wang, J.W. Cui, Q. Zhang, L.P. Yang and Y.C. Wu, *J. Mater. Chem. A*, 7 (2019) 4998.
38. M. Mirzaee, C. Dehghanian, *J. Solid State Electr.*, 22 (2018) 3639.
39. Z.M. Hu, X. Xiao, C. Chen, T.Q. Li, L. Huang, C.F. Zhang, J. Su, L. Miao, J.J. Jiang, Y.R. Zhang, and J. Zhou, *Nano Energy*, 11 (2015) 226.
40. S. Eugénio, T. M. Silva, M.J. Carmezim, R.G. Duarte and M. F. Montemor. *J. Appl. Electrochem.*, 44 (2014) 455.
41. P. Wen, P.W. Gong, J.F. Sun, J.Q. Wang and S.R. Yang, *J. Mater. Chem. A*, 3 (2015) 13874.
42. S. Parwaiz, K. Bhunia, A.K. Das, M.M. Khan and D. Pradhan, *J. Phys. Chem. C*, 121 (2017) 20165.
43. A.K. Mishra, A.K. Nayak, A.K. Das and D. Pradhan, *J. Phys. Chem. C*, 122 (2018) 11249.
44. S.S. Wu, W.F. Chen, L.F. Yan, *J. Mater. Chem. A*, 2 (2014) 2765.